Sensitive, Automated, and Web-aware Interferometers With Unified Analysis of F-region Dynamics at Upper Atmospheric Facilities

R.B. Kerr, J. Noto, J. Riccobono, M. Migliozzi, and S. Kapali

Scientific Solutions, Inc., North Chelmsford, MA

Array detection permitting field-widened multiplexing of the Fabry-Perot interference pattern has increased OI red line sensitivity more than 30-fold at the Millstone Hill Optical Facility in Westford, MA. Perhaps more importantly, automated data taking produces thermospheric winds and temperatures every clear night of any month, with calibration and data taking control from any web connection, or by defining and scheduling events to control the system instruments and acquire data. This capability, producing neutral meridional and zonal wind vectors with 1 m/s errors in 8 minutes, and thermospheric neutral temperatures with statistical errors <15K in 4 minutes, in the quietest of conditions. Our analysis algorithm begins with raw CCD images, followed by application of automated flat field and dark current corrections and consistent anomalous pixel filtering, and proceeds to the summation of five Fabry-Perot interference orders following Fourier decomposition of the instrument function in each order. This algorithm is applied without user intervention, and is now prepared for real time applications. Uniform application of these instrument automation and analysis techniques should provide a reliable and chain-consistent neutral wind and tem-

The Physics of Neutral Winds

The emissions of interest are produced by a metastable state of oxygen, O^1D, decaying via a forbidden transition from the $^1D_2$ to the $^3P_1$ state. In the nighttime atmosphere, these emissions come from a very specific layer, located below the F-region peak ~ 210-225 km altitude, in the thermosphere. Neutral winds are generated (primarily) by pressure gradients caused by dayside solar heating.

- During the day winds are poleward/westward
- During the night winds are Equatorward/ eastward
- Decrease in magnitude with increasing solar activity due to increased ion drag.
- High latitude magnetospheric convection can influence mid-latitude winds. *[Emmert et al.]*

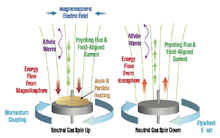

Figure courtesy of Jeff Thayer

This Project:

- Upgraded & automated the existing 6300Å FPI at Millstone Hill.
- Adds a dedicated 5577Å FPI.
- observes 6300Å & 5577Å automatically.
- Provides temperature and wind data to the Madrigal database.

Optical Layout

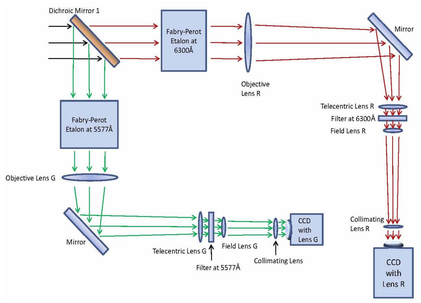

Optical configuration for the completed Millstone Hill interferometer light enters the instrument via a pointing head. It is then separated by a dichroic mirror into light with a wavelength greater than 6000Å and light with a wavelength shorter than 6000Å. The "red" light passes straight through and the "green" light is folded by 90 degrees. After passing through the appropriate etalon a series of lenses are used to image the fringe pattern telecentrically onto an interference filter. Then it passes through a field lens, collimator, and finally a camera lens is used to re-image the fringe pattern onto a CCD camera. The red "arm" is fully functional the green "arm" will be operation by summer.

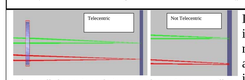

The small change in angle in a non-telecentric system will increase "walk-off" or change in the width of the instrument function towards the edge of the FOV.

In a telecentric optical system, all of the rays incident on the filter are parallel to the chief ray and are incident on the filter at the same angle. This removes center-to-edge variation in the width of the fringes caused by the varying angle of incidence in a collimated system.

The Scientific Solutions Millstone Hill Fabry-Pérot Interferometer

The Millstone Hill Doppler Imaging FPI, layout left, is an f/13.8 system, with 10.16 cm clear aperture and a 140 cm effective focal length. The 50.8mm 6300Å interference filter is 4.0Å broad, in a telecentric optical configuration that relieves the requirement for image-quality filtering. Cosmetic filter defects are removed by flat-field calibration. The etalon system is an air-gap, with 1.0525 cm spacing. This provides a 0.1886Å free spectral range at 6300Å, and a typical spectral resolution of 0.021Å. Five orders of the 6300Å airglow emission are sampled simultaneously from a 2° field-of-view with an Andor DW436 camera featuring a 2048x2048 E2V42-40 back illuminated CCD. This detector has a quantum efficiency of 75% at 6300Å, with dark noise of 0.00024 $e^- s^{-1}$ pixel at -76^{0}C. Typical instrument performance produces 6300Å wind vectors with accuracies of approximately ± 2 m/s and temperatures with accuracies of ±15K using four-minute exposure times. Exposure times can be enhanced to reduce temperature errors, or reduced to improve time resolution of wind vectors. We use 1.0525 cm spacers for the airglow observations because Dwight Sipler determined that this precise gap size would force nearby OH Meinel emissions to appear in the OI 6300 Å background.

Interferometer Summary

Aperture:	100 mm	Vectors every 4 minutes
FSR:	0.0189 nm	Operates 21-26 days
Finesse:	~9	per month
CWL:	6300 Å	Data on Madrigal
Error+/-:1.5 m/s &	10^0	

Calibration System

Instrument calibration is achieved using two different calibration sources. First a low brightness white light source consisting of a tungsten bulb and a diffuser box is used to "flat field" the system. A frequency stabilized Helium Neon (HeNe) laser is used to measure the instrument width of the Fabry-Perot system. Flat fields and laser calibration images are collected several times nightly. Both the red and green arms will be calibrated with the same HeNe laser.

Determining the flat-field of the instrument is done as often as necessary. Flat fields are quite stable, as long as the instrument configuration is stable. The flat field calibration of the instrument is obtained by shining a light through a light diffuser box that is permanently installed above the instrument and fills the field-of-view of the instrument. An image of that uniform source of light is obtained with all components in the optical path of the instrument so that any imaging artifacts from the optical system can be removed from the data.

This drawing illustrates our flat field calibration box. Broadband light is introduced at the bottom of the box with a fiber optic cable that is connected to an incandescent source. That fiber entry port is illustrated at the bottom of the drawing on the left. The diffuse light beam is further dispersed by a diffusing hemisphere, and the box output passed through two diffusing screens at the top. The FPI mirror system looks in the nadir to view this flat field light source. All inner surfaces of the flat field box are painted flat white.

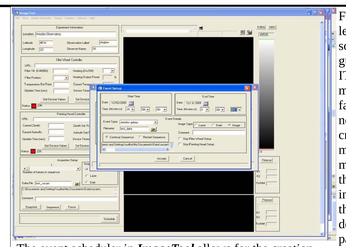

For interferometer operation ***ImageTool***, Figure left, has been created using a combination of software development tools. The primary language is Interactive Data Language (IDL) from ITT Visual Solutions; this allows rapid implementation of a graphical and user friendly interface that is system independent. Using a technology licensed from Bruxton Corp., SSI has created a single application that can control multiple CCD cameras using a simple pull down menu. A powerful scheduling utility was created that allows the user to create and save multiple independent observing events or modes utilizing the pointing head, filter wheel, and any selected device. ***ImageTool*** is also Internet aware and capable of remote observing sessions.

The event scheduler in ***ImageTool*** allows for the creation and automatic execution of complex observing modes or events, including following the shadow height of a resonant emission, various wind modes, or moving away from contaminating galactic sources.

Finding Ring Center

Center finding is based on the fact that three Cartesian points define a circle. The algorithm begins at azimuth positions 0º, 120º , and 240º on the FPI ring pattern, and marches out from an initial guess line center along each azimuth direction searching for a maximum signal level. The three maxima define a circle with a determined central Cartesian value. The determination is repeated in 1º azimuth intervals around the ring pattern, until 120 determinations are made. The median value (to preclude outliers from weighting a mean) of these 120 determinations is assigned as ring center for a laser image. This process is performed on every laser image acquired during a night, and the median of these samples is the final ring center. If only two lasers images are acquired, the 2nd laser sample center is assigned ring center, if only one laser is sampled that sample provides ring center. This center finding procedure is very robust, the algorithm defines ring center to a fraction of a pixel.

Automated Analysis Technique to Extract Geophysical Parameters

Next Generation: Synchronized imaging on multiple systems

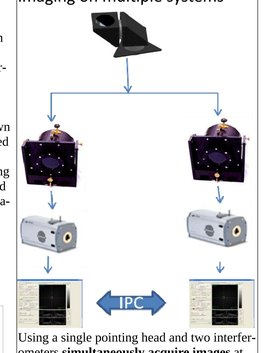

Using a single pointing head and two interferometers **simultaneously acquire images** at different wavelengths. **Synchronized acquisition** realized through inter-process communication between multiple instances of ImageTool on the network.

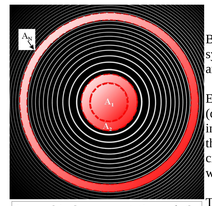

Ring Summing

Because the fringe pattern of a Fabry-Pérot etalon is azimuthally symmetric, the pattern can be summed in annular sections of equal area to smooth out variations and increase signal-to-noise.

Each annulus represents a spectral resolution element of the pattern (dl). Because the annuli are of equal area, their width decreases moving away from the center. The radius of the Nth annulus is related to the radius of the first by $r_N = (\sqrt{N})r_1$. The outer annulus should coincide with the outermost fringe, and be wide enough to have sufficient width, in pixels, to Nyquist-sample that outermost fringe.

A graphical representation of the equal-area resolution elements over which annular summing takes place. All of the areas are equal. The Hadinger fringe pattern is a HeNe laser pattern from a single etalon

To achieve maximum signal-to-noise ratio for the Fabry-Perot, the counts from an entire ring are added together. The sum then becomes the total number of counts at the radial position of that resolution element ring. The total number of counts at each radial position are then plotted sequentially as a high signal-to-noise radial graph of intensity. It is conceptually similar to taking a radial slice through the Fabry-Perot fringe pattern, except all the spectrally equivalent pixels from each ring have been placed along that line, collapsing (or, in topological terms, degenerating) each ring to a point on that radial line.

Removing Instrument Drift

Maintaining the pressure in the etalon pressure pot is integral to achieving the spectral stability of this instrument, and is controlled by a pressure servo. This servo is a standard component used in other SSI airglow systems. Pressure is measured in each etalon pressure pot using a pressure transducer. As the pressure drifts, the pressure servo uses a servo motor to open and close a needle valve which is fed from a high pressure (50 psi) nitrogen reservoir. A PID algorithm is used to control the rate that the valve is opened or closed allowing for pressure control to 0.01 PSI, easily compensating for any small leakage.

Each pressure servo has an on-board microcontroller that communicates to the control computer via the RS-232 protocol. The FP control system uses this information to guarantee that the ring pattern center is at a background spectral position. Thermal control of the etalon units in each pressure pot is achieved using a thermistor, resistive heater and a PID controller.

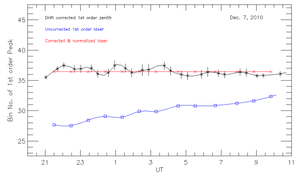

Our ideal data taking scheme is to take laser calibration exposures throughout the night, interspersed after two cycles of N, S, E, W, zenith mirror pointing cycles on the sky. These laser calibrations allow us to track any spectral drift that may occur in the instrument during a night, and thus permit the extraction of vertical winds relative to a nightly average.

The correction process first finds the average bin position of the 1st order laser line center, and normalizes that value to the average of the zenith sky measurements 1st order line center values. All laser line center values are adjusted by that same normalization factor. The line center of each laser sample is then corrected with an additive term that makes the laser center bin position constant throughout the night – as it would be without instrument drift. The line center position of all other spectra sampled during the night, in any direction, are corrected by spline interpolation of the correction term from the time series of laser corrections. The figure above illustrates this drift correction process.

The image on the left is a single, raw, dark image. The image on the right is the sigma filtered, median filtered image before averaging all of the pixels.

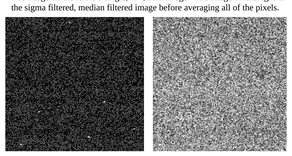

Median Filtering

Dark images are acquired with the camera shutter and roof shutter closed, and with all room lights extinguished. These are acquired with exposure times equal to that used to acquire images on the sky. Each dark image is sigma-filtered in 8 X 8 pixel blocks setting pixels within to the average if they exceed the average by more than 3-sigma. The process is iterated until no such pixels exist. This eliminates hot or dark pixels. Then, if there are more than 5 dark samples, a median filter is applied over all the samples to eliminate random bright pixels caused by cosmic ray hits in the determined dark image. If there are fewer than 5 dark frames available, an average of these is used. Finally, an average dark frame is determined by averaging the signal over all pixels of the processed dark image and assigning that value to each pixel. This average dark frame is stored for all subsequent dark subtractions.

The image on the left below is a raw, single flat field image. The image on the right is the sigma filtered, median filtered, optical beam-only flat field prior to normalization for flat field correction.

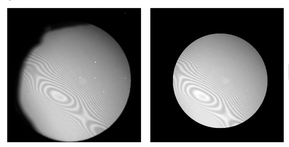

Flat Fielding

To remove hot or dark pixels, individual flat field images are first sigma filtered within 12 X 12 pixel boxes with the average therein assigned to any pixel 3 -sigma different from the average. The filtering is iterative until no pixel is 3-sigma beyond the mean. A median filter defines the flat image when there are more than 5 image samples, and an average is used if less than 6 samples are available.
Our optical beam does not cover the entire CCD array, and consequently a more reliable flat field image is determined (a more sensitive image) if the sigma filter and the median filtering are applied only to the pixels within the optical beam. As such, the flat field analysis is applied only in a region containing the optical beam, with all other pixels outside the beam set to a value of 1.0 (dark). The final flat field image is formed by the median filtered image with the average dark image subtracted.

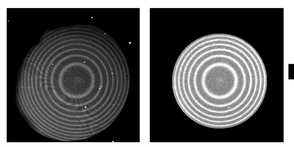

Sky image processing.

Each image containing sky airglow data is first sigma filtered to remove hot and dark pixels, using 8 X 8 pixel regions, with pixel values set to that region's mean if the pixel exceeds the mean by more than 2.5 standard deviations. This filter iterates until no pixel in the image exceeds 2.5 sigma of its nearby population. Then, the average dark image is subtracted from the filtered sky image, and the median filtered, normalized flat field image is divided into the sky image to perform the flat field correction. Finally, the image is restricted to the region of the optical beam, with all other pixels set to equal 1.0 (dark). The two figures above illustrates a raw sky airglow image, and the processed version of that image.

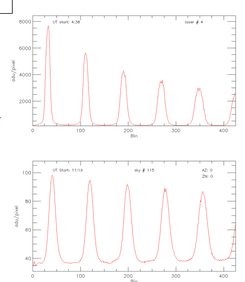

Bin Summing

Both laser calibration images and sky images are bin summed. The bin summing algorithm follows that developed by the University of Wisconsin Aeronomy group *Coakley*, [1995] and *Mierkiewicz*, [2006]. Annuli of equal pixel area around ring center are established with a radius maximum and a delta pixel width, such that each annulus has an equal area, and signal is summed within each annulus. This algorithm converts the radially symmetric FPI fringe pattern, sampled on the Cartesian CCD, to linear wavelength bins. The figures above illustrates a bin summed spectra of a laser image (top), and a sky airglow image (bottom).

The top panel illustrates a fit to a laser calibration spectrum. Bin summed data are illustrated with blue "x" data points. The middle panel shows sky data with red x data points, and a multiple Gaussian function corresponding to initial guess parameters overlayed with the solid black line. The bottom panel is the completed nonlinear least squares Gaussian fit to the data in the middle panel. In this bottom panel, the data are shown with blue x data points, and the fit is overlain with a solid black line.

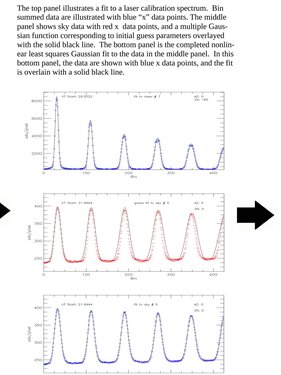

Gaussian Fit

Each laser and sky 5-order bin summed spectrum is fit to a Gaussian function using the Levenberg-Marquardt nonlinear least squares fitting algorithm developed by *Moré*, [1978], *Moré, & Wright*, [1993], and *Markwardt*, [2008]. In fact, a six Gaussian "user supplied" function is supplied to the fitting algorithm, though only 5 FPI orders are used for the analysis. The optical beam domain established in the imaging processing is defined to include 6 orders and their backgrounds (Figure above). Similarly, the maximum pixel radius to be included in the bin sums is defined to include 6 orders. We fit a 6 Gaussian function because that selection serves to stabilize the background fit in the 5th order – the last order included in our spectral analysis.

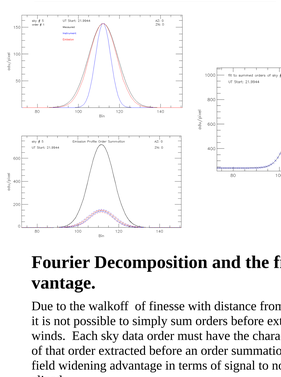

Fourier Decomposition and the field widening advantage.

Due to the walkoff of finesse with distance from the center of the optical axis, it is not possible to simply sum orders before extraction of temperatures or winds. Each sky data order must have the characteristic instrument function of that order extracted before an order summation – and full realization of the field widening advantage in terms of signal to noise improvement – can be realized.

To sum five orders of the sky data in each ring pattern exposure, we perform a Fourier decomposition of the instrument function (measured using the frequency stabilized HeNe laser data). Each sky FPI order and each laser calibration order (using laser samples made closest in time to the sky sample) is redefined on a 1 FSR grid centered on the bin number of its Gaussian line center. A fast Fourier transform is then applied to the each sky and laser order, and division of the sky transform by the laser transform produces the decomposed emission function in frequency space. The inverse transform produces the emission function in each order, and these are then summed (after each is shifted to have a line center position equal to the 1st order line center position) to gather every photon in the field widened airglow image. In this process, the Gaussian fit to the proper laser order is normalized to the amplitude of the corresponding sky order, but the amplitude of the sky order is preserved. Background is removed by subtraction.

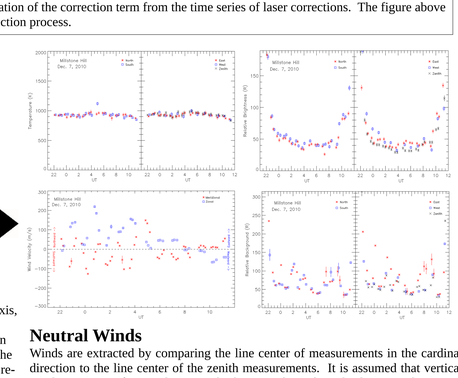

Neutral Winds

Winds are extracted by comparing the line center of measurements in the cardinal direction to the line center of the zenith measurements. It is assumed that vertical winds are insignificant relative to the horizontal winds and relative to the instrument spectral resolution. Line-of-sight winds are calculated by subtracting the line center bin position in a cardinal direction from the zenith center position interpolated in time to match the observation time at the cardinal point. (The zenith line center position is monitored throughout the night, and does not remain precisely constant, due either to the presence of small vertical winds, or to slight thermal instrument drift, or both.) These line-of-sight vectors are cosine-corrected to lie in the emitting layer, and use the convention of positive northward and positive eastward. Meridional [zonal] winds are calculated by summing the North-South [East-West] line-of-sight vectors and dividing by two. Each North or South [East of West] measurement creates a meridional [zonal] vector by interpolating the corresponding South or North [West of East] vector corresponding to the time of the North or South [East of West] observation. Meridional [zonal] gradients, South-to-North [West-to-East] are calculated by subtracting the North [East] line-of-sight vector from the South [West] line-of sight vector, and dividing by the distance between the two emission regions, which is established by the emission height and the observation zenith angle.

Acknowledgements

This work has been supported by the National Science Foundation's Aeronomy program, grants #ATM 0437343, ATM 0640560 & AGS 0940257.

www.neutralwinds.com

References

Coakley, Monica M., *Application of the CCD Fabry-Pérot Annular Summing Technique to Thermospheric O'D*, Ph. D. Thesis, 1995

Emmert, J. T., B. G. Fejer, and D. P. Sipler, Climatology and latitudinal gradients of quiet time thermospheric neutral winds over Millstone Hill from Fabry-Perot interferometer measurements, J. Geophys. Res., 108 (A5), 1196, doi:10.1029/2002JA009765,2003.

Markwardt, C. B. 2008, "Non-Linear Least Squares Fitting in IDL with MPFIT," in proc. *Astronomical Data Analysis Software and Systems XVIII*, Quebec, Canada, ASP Conference Series, Vol. 411, eds. D. Bohlender, P. Dowler & D. Durand (Astronomical Society of the Pacific: San Francisco), p. 251-254 (ISBN: 978-1-58381-702-5)

Mierkiewicz, E.J., F.L. Roesler, S.M. Nossal & R.J. Reynolds (2006), "Geocoronal Hydrogen Studies Using Fabry-Perot Interferometers, Part 1: Instrumentation, Observations, and Analysis," Journal of Atmospheric & Solar-Terrestrial Physics, 68, 1520, doi:10.1016/j.jastp.2005.08.024

Moré, J. 1978, "The Levenberg-Marquardt Algorithm: Implementation and Theory," in *Numerical Analysis*, vol. 630, ed. G. A. Watson (Springer-Verlag: Berlin), p. 105

Moré, J. & Wright, S. 1993, "Optimization Software Guide," SIAM, *Frontiers in Applied Mathematics*, Number 14. (ISBN: 978-0-898713-22-0)

MINPACK-1, Jorge More', available from netlib. http://www.netlib.org/minpack